Contents lists available at ScienceDirect

Journal of Membrane Science

journal homepage: www.elsevier.com/locate/memsci

Fouling mechanisms in constant flux crossflow ultrafiltration

Alon Y. Kirschner[a,1], Yu-Heng Cheng[a,1], Donald R. Paul[a], Robert W. Field[b,*], Benny D. Freeman[a,*]

[a] University of Texas at Austin, Department of Chemical Engineering, Texas Materials Institute, Center for Energy and Environmental Resources, and Environmental and Water Resources Engineering, 10100 Burnet Road, Building 133, Austin, TX 78758, USA
[b] University of Oxford, Department of Engineering Science, Parks Road, Oxford OX1 3PJ, UK

ARTICLE INFO

Keywords:
Ultrafiltration
Threshold flux
Fouling
Crossflow
Constant flux

ABSTRACT

Four fouling models due to Hermia (complete pore blocking, intermediate pore blocking, cake filtration and standard pore blocking), have long been used to describe membrane filtration and fouling in constant trans-membrane pressure (ΔP) operation of membranes. A few studies apply these models to constant flux dead-end filtration systems. However, these models have not been reported for constant flux crossflow filtration, despite the frequent use of this mode of membrane operation in practical applications. We report derivation of these models for constant flux crossflow filtration. Of the four models, complete pore blocking and standard pore blocking were deemed inapplicable due to contradicting assumptions and relevance, respectively. Constant flux crossflow fouling experiments of dilute latex bead suspensions and soybean oil emulsions were conducted on commercial poly (ether sulfone) flat sheet ultrafiltration membranes to explore the models' abilities to describe such data. A model combining intermediate pore blocking and cake filtration appeared to give the best agreement with the experimental data. Below the threshold flux, both the intermediate pore blocking model and the combined model fit the data well. As permeate flux approached and passed the threshold flux, the combined model was required for accurate fits. Based on this observation, a physical interpretation of the threshold flux is proposed: the threshold flux is the flux below which cake buildup is negligible and above which cake filtration becomes the dominant fouling mechanism.

1. Introduction

Modeling membrane fouling has played an integral part in advancing our understanding of membrane separation processes. Hermia developed equations to describe four distinct fouling mechanisms in constant pressure dead-end filtration (DEF): complete pore blocking, intermediate pore blocking, standard pore blocking, and cake filtration [1]. Bowen used these models to identify the dominant fouling mechanism at different stages of microfiltration membrane fouling during BSA filtration [2]. Ho and Zydney combined the pore blocking and cake filtration mechanisms to accurately describe bovine serum albumin (BSA) protein fouling during microfiltration [3]. Field et al. further developed Hermia's basic models to include a foulant removal term applicable in crossflow (XFLOW) filtration [4,5]. Hlavacek and Bouchet developed equations for the complete, intermediate and standard pore blocking mechanisms for constant flux dead-end filtration [6]. These models were applied to BSA microfiltration experiments, and the intermediate pore blocking model gave the best agreement with experimental data. Ho and Zydney also developed a combined model for pore blocking and cake filtration in constant flux dead-end microfiltration and used it to describe BSA protein fouling [7]. Bolton et al. developed five different combined models for constant pressure and constant flux dead-end filtration, each incorporating two fouling mechanisms [8]. A combined complete pore blocking and cake filtration model provided the best agreement with results from immunoglobulin G (IgG) and BSA filtration experiments. However, this model was not able to identify these as the actual fouling mechanisms. These models do not account for possible foulant removal due to crossflow shearing forces, and therefore cannot describe constant flux crossflow filtration. Modeling of fouling mechanisms in constant flux crossflow filtration is scarce, despite the fact that many practical membrane separations are conducted in this fashion [9].

This study presents a re-development of Hermia's equations to describe **constant flux crossflow filtration**. Experimental results for constant flux crossflow ultrafiltration (UF) of a latex bead suspension, taken to be a rigid foulant, were compared to the models, and applicability of the models is discussed. Additionally, a soybean oil-in-water emulsion was used to represent deformable foulants. A model

* Corresponding authors.
E-mail addresses: robert.field@eng.ox.ac.uk (R.W. Field), freeman@che.utexas.edu (B.D. Freeman).
[1] Co-first authors.

https://doi.org/10.1016/j.memsci.2018.12.001
Received 12 September 2018; Received in revised form 29 November 2018; Accepted 1 December 2018

Nomenclature

a	Unobstructed membrane surface area [m^2]
B	Particle resuspension rate [s^{-1}]
C	Volume of solid particles retained per unit filtrate volume
C_p	Organic carbon concentration in the permeate [mg/L]
C_f	Organic carbon concentration in the feed [mg/L]
J	Permeate flux [m/s]
K_j	Constant depending on fouling mechanism: j = i (intermediate), s (standard), c (cake)
L	Pore length (membrane thickness) [m]
m	Mass ratio of wet to dry cake
n	Step number in flux stepping experiment
N	Number of membrane pores
ΔP	Transmembrane pressure [N/m^2]
Q	Volumetric flow rate [m^3/s]
R	Overall filter resistance [m^{-1}]
r	Pore radius [m]
s	Mass fraction of solids in the fouling solution
S	Rate of erosion of cake per unit area [$kg/(m^2\ s)$]
t	Filtration time [s]
t*	time at which the intermediate pore blocking stage is predicted to end [s]
TF	Threshold flux [$L/(m^2 \cdot h)$]
V	Filtrate volume [m^3]
W	Cake mass [kg]
α	Cake specific resistance [m/kg]
γ	Filtrate density [kg/m^3]
	fluid viscosity [$N\ s/m^2$]
σ	Blocked area per unit filtrate volume [m^{-1}]
Superscript - X^N	Superscript N indicates the step number that parameter X is being examined at, where X can be K_j, ΔP_0, J, permeance, or *t*.

combining intermediate pore blocking and cake filtration was used to model the progression of fouling in these experiments.

The threshold flux (TF) was defined by Field and Pearce as "useful to distinguish between regions of low fouling and high fouling both in direct-flow and crossflow systems" [10]. Thus far, the TF has been useful as a tool to characterize and compare the fouling resistance of different membranes, but it has not been defined in physical terms [11–13]. Based on the proposed models, a physical interpretation of the TF is suggested, which clarifies the transition between different fouling mechanisms occurring at the tipping point between slow and rapid fouling.

2. Theoretical background

2.1. Membrane operating modes

Filtration in a membrane system is often categorized as either dead-end or crossflow [14]. In dead-end filtration (cf., Fig. 1a), the feed flow is perpendicular to the membrane surface. Rejected foulants accumulate on or near the membrane surface, and have no path to exit the system (hence "dead-end"). In crossflow filtration (cf., Fig. 1b), the feed flow is tangential to the membrane surface. Consequently, the shear flow can transport rejected foulants out of the system, mitigating fouling and concentration polarization [14]. Typically, either transmembrane pressure or permeate flux are held constant. Therefore, most membrane operations fall into one of four categories:

1. constant ΔP dead-end filtration, 2. constant ΔP crossflow filtration, 3. constant flux dead-end filtration, or 4. constant flux crossflow filtration.

2.2. Fouling mechanisms

Hermia's fouling models have several fundamental assumptions: 1. constant pressure dead-end filtration, 2. membrane pores are cylindrical, parallel to each other, and uniform in diameter, and 3. foulant particles are uniform, non-deformable spheres [1]. These assumptions enable a simple mathematical description of four distinct fouling mechanisms. Each mechanism has its own unique assumptions in addition to those outlined above. *Complete pore blocking* (cf., Fig. 2a) assumes that fouling is a surface phenomenon, where foulant particles deposit onto unobstructed surface areas (completely blocking the pores in the covered area), but do not deposit on top of each other [1]. *Intermediate pore blocking* (cf., Fig. 2b) is similar to complete pore blocking, but particles are permitted to deposit on top of each other. Each foulant has a probability to either deposit on an unobstructed area of the membrane or deposit onto a previously deposited foulant particle [1]. The overall filter mass transfer resistance is defined as the sum of the membrane resistance and the cake resistance, where the cake is the layers of particles deposited on the membrane surface. In his derivation of complete and intermediate pore blocking, Hermia assumed negligible cake growth, attributing permeate flux decline to a reduction in open pore area, so overall filter mass transfer resistance was taken to be constant [1]. In *cake filtration* (cf., Fig. 2c), foulants completely cover a membrane surface in several layers. In this case, the cake covers the entire membrane surface area, and the overall filter mass transfer resistance increases in proportion to the cake layer thickness [1]. Finally, *standard pore blocking* (cf., Fig. 2d) is fundamentally different, assuming that blocking occurs only inside the pores, where deposited particles reduce the pore diameter [1].

3. Model development

The equations derived below are appropriate for constant flux crossflow filtration. In crossflow filtration, shear force from the feed flow may remove foulants from the membrane surface [15]. Therefore, a foulant removal term is incorporated in the surface fouling mechanisms (*i.e.,* complete pore blocking, intermediate pore blocking, and cake filtration). Standard pore blocking is not a surface phenomenon, so addition of crossflow should not affect this fouling mechanism [4].

The derivation below closely follows Hermia's model development for constant ΔP dead-end filtration and Field et al.'s modification to include a crossflow foulant removal term [1,5]. Adjustments are made for constant flux operation. Constant flux refers to the total permeate flux through the membrane. As the membrane fouls, the open pore area decreases, causing the local flux through some pores to decrease, while

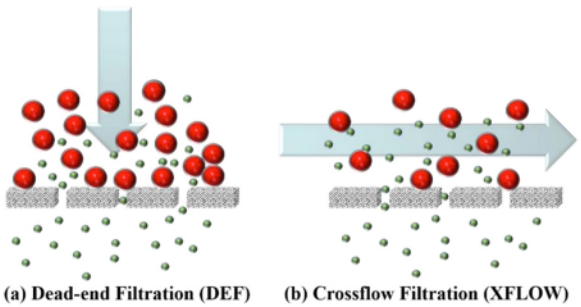

Fig. 1. Main flow types in membrane separations: (a) Dead-end filtration and (b) Crossflow filtration. Large (red) spheres represent rejected particles, small (green) spheres represent non-rejected particles, and the arrows indicate the feed flow direction. (For interpretation of the references to colour in this figure legend, the reader is referred to the web version of this article.)

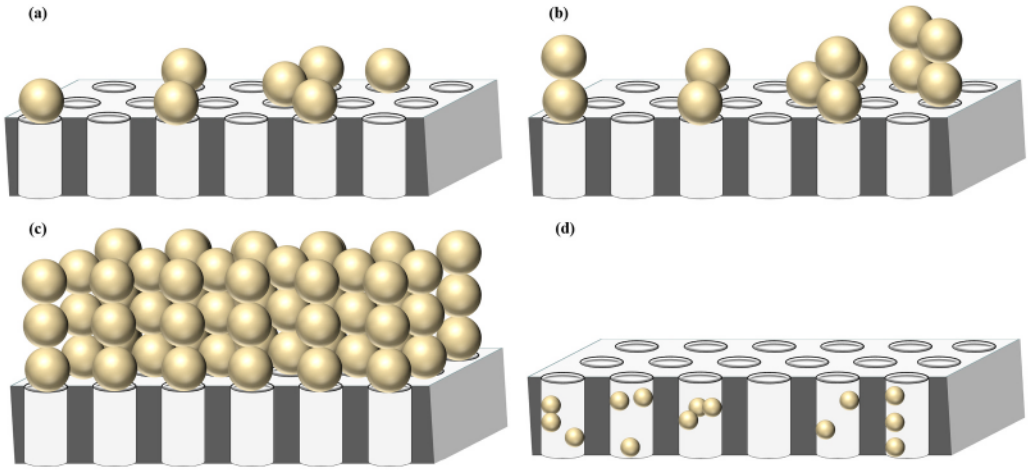

Fig. 2. Schematic representation of Hermia's fouling mechanisms: (a) Complete pore blocking, (b) Intermediate pore blocking, (c) Cake filtration and (d) Standard pore blocking [1].

the flow through others increases to compensate. However, at all times the total flux through the entire membrane is constant [16]. A summary of the ΔP relations for all four fouling mechanisms is provided in Table 1.

3.1. Complete pore blocking

According to Darcy's Law for flow through a porous membrane [1]:

$$Q \quad \frac{\Delta \ a}{\mu R} \tag{1}$$

where Q is the volumetric flow rate [m^3/s], ΔP is transmembrane pressure [N/m^2], is the unobstructed (clean, unfouled) membrane surface area [m^2], μ is the fluid viscosity [$N{\cdot}s/m^2$], and R is the overall filter mass transfer resistance [m^{-1}].

For constant flux, Q at time t = 0 (Q_0) should equal Q at all other times (Q_t). Following Hermia's approach, the overall filter resistance is assumed to be constant, attributing the increase in ΔP during fouling to a reduction in unobstructed membrane surface area. Therefore, comparing the expressions for Q_0 and Q_t from Eq. (1):

$$\Delta_{\ t} \quad \frac{\Delta \ a}{a_t} \tag{2}$$

where the subscripts 0 and t reflect initial conditions and conditions at time t, respectively.

From Hermia, the unobstructed membrane surface area in complete pore blocking is a function of the filtered volume of solution [1]:

$$a_t \quad a \ - \sigma \tag{3}$$

where V is the filtrate (*i.e.*, permeate) volume [m^3] that has passed through the membrane, and σ is the blocked membrane surface area per unit filtrate volume [m^{-1}].

In constant flux operation, the permeation rate will not change, and V can be expressed as the product of the initial flowrate and the filtration time:

$$V \quad Q \ t \quad a \ \ t \tag{4}$$

where J is the permeate flux [m/s].

Substituting Eq. (4) into Eq. (3) and rearranging gives:

$$-\frac{da}{dt} \quad \sigma a \tag{5}$$

Based on Field et al., when accounting for crossflow, the rate of change in unobstructed membrane surface area is a function of two counteracting processes: foulant deposition and foulant removal [4,5]. Foulant removal is taken to be proportional to the blocked filtration area [5]. If particles are removed at a constant rate from blocked pores, the decrease in unobstructed membrane surface area is given by [5]:

$$-\frac{da}{dt} \quad \sigma a \ J - \left(a \ - a\right) \tag{6}$$

where B is the particle resuspension rate, a constant reflecting the frequency at which foulants are removed from the membrane surface by the crossflow shear force [s^{-1}]. The first term on the right-hand side of Eq. (6) is the foulant deposition term, and the second term is the foulant removal term.

Integration of Eq. (6) yields an expression for the unobstructed membrane surface area as a function of time:

$$a_t \quad a \left(1 - \frac{\sigma J}{}\left(1 - \exp\left(- \ t\right)\right)\right) \tag{7}$$

Substituting Eq. (7) into Eq. (2) results in:

$$\Delta P_t \quad \frac{\Delta P_0}{1 - \frac{\sigma J}{} \ 1 - \exp \ - \ t))\Big)} \tag{8}$$

which is the time dependence of ΔP for complete pore blocking.

The unobstructed membrane surface area decreases as pores are blocked during fouling. Physical limitations (*i.e.*, a_t must always be positive and equal to or less than a_0) require the second term in parentheses in Eq. (7) to always lie between 0 and 1. Therefore, the term $\frac{\sigma J}{}$ is always less than or equal to 1 in complete pore blocking.

When the second term in the denominator of Eq. (8), $\frac{\sigma J}{} \ 1 - \exp \ - \ t))$, is between 0 and 1, the model predicts a rise in ΔP with time. When this term equals 1, all pores have been blocked, and ΔP

Table 1
Summary of the relationships between ΔP and filtration time for the four proposed fouling mechanisms in constant permeate flux crossflow filtration.

Complete	Intermediate	Cake	Standard
$\Delta P_t \quad \frac{\Delta P_0}{\left(1 - \frac{\sigma J}{} \ 1 - \exp \ - \ t)\right)}$	$\Delta P_t = \frac{\Delta P_0}{\left(\frac{1}{K_i} \ \left(1 - \frac{1}{K_i}\right)\exp \ -K_i \ t)\right)}$	$\Delta P_t = \Delta P_0 \ 1 \quad K_c \ t)$	$\Delta P_t \quad \frac{\Delta P_0}{1 - K_s a_0 \ t)^2}$

increases to infinity.

In Hermia's development, complete pore blocking was a reasonable mechanism for constant ΔP operation. Even when all pores are blocked, a constant ΔP can still be applied (the permeate flowrate simply declines to zero). However, assuming constant flux with all pores completely blocked is not realistic. Under certain conditions, complete pore blocking predicts similar ΔP profiles as intermediate pore blocking (cf., Fig. S1a in the Supporting information (SI)), but it is not universally applicable to those situations where constant flux crossflow is observed to be a reality.

3.2. Intermediate pore blocking

Following Hermia's development, the probability for a particle to deposit onto an open pore, rather than on a previously deposited particle, is proportional to the instantaneous unobstructed membrane surface area [1]. The rate of change of unobstructed membrane surface area, based on Eq. (5), is expressed by:

$$-\frac{da}{dt} \quad \sigma a \tag{9}$$

The only difference between Eq. (9) and Eq. (5) is the area accounted for on the right-hand side of the equation. In intermediate pore blocking, each foulant particle has a probability to either block an open pore or deposit on a previously deposited foulant particle [1]. The probability of blocking an open pore decreases as additional pores are blocked. Therefore, to account for the decreasing blocking rate during fouling, σa from Eq. (5) is changed to σa

In crossflow filtration, the foulant removal term is identical to that introduced for complete pore blocking (cf., Eq. (6)):

$$-\frac{da}{dt} \quad \sigma aJ - \left(a \quad - a\right) \tag{10}$$

Integration of Eq. (10) yields the following expression for the unobstructed membrane surface area as a function of time:

$$a_t = a\left(\frac{1}{K_i} \quad \left(1 - \frac{1}{K_i}\right)\exp\left(-K_i \quad t\right)\right) \tag{11}$$

where K_i is the intermediate pore blocking constant for crossflow filtration and is defined as:

$$K_i = \frac{\sigma J}{} \tag{12}$$

Substitution of Eq. (11) into Eq. (2) results in:

$$\Delta P_t = \frac{\Delta P_0}{\left(\frac{1}{K_i} \quad 1 - \frac{1}{K_i}\right)\exp\left(-K_i \quad t\right)\right)} \tag{13}$$

which is the time dependence of ΔP for intermediate pore blocking.

Eq. (13) reveals no inconsistencies in constant flux operations like those found for complete pore blocking. The denominator of this equation is always positive, with a minimum value of $1/K_i$ and a maximum value of 1. The equation predicts an initial rise in ΔP, plateauing at long times to a constant value: $\Delta P_{t\to\infty} \quad \Delta P_o \quad _i$ (cf., Fig. 3Sa in the SI). The plateau in ΔP results from the decreasing probability of a foulant particle blocking an open pore as more and more pores are blocked. A balance between particle deposition and particle removal is reached, and the constant flux assumption is not violated.

3.3. Cake filtration

In cake filtration, the overall filter resistance is expressed as the sum of the clean membrane resistance and the resistance of the deposited foulant layers [1]. An erosion term is added to account for removal of foulant layers due to crossflow [4]:

$$_t = \frac{\alpha W}{a} - \alpha St \tag{14}$$

where α is the cake specific resistance [m/kg], W is the cake mass [kg] and S is the rate of erosion of cake per unit area [kg/(m^2 s)], which is assumed to be invariant with time [4].

From a mass balance on the cake [1,17]:

$$W \quad \frac{\gamma s}{1 - ms)} \tag{15}$$

where γ is the filtrate density [kg/m^3], s is the mass fraction of solids in the fouling solution, and m is the mass ratio of wet to dry cake.

Substitution of Eq. (4) and Eq. (15) into Eq. (14) results in an expression for overall filter resistance as a function of time:

$$R_t = R_0 \quad 1 \quad K_c \quad t) \tag{16}$$

where K_c is the cake filtration constant for crossflow filtration [m^{-1}], defined as:

$$K_c \quad \frac{\alpha\gamma s}{R_0 \quad 1 - ms)} - \frac{\alpha S}{R_o} \tag{17}$$

Substitution of Eq. (16) into Darcy's Law (Eq. (1)) yields:

$$\Delta P_t = \Delta P_0 \quad 1 \quad K_c \quad t) \tag{18}$$

which is the time dependence of ΔP for cake filtration.

Eq. (18) predicts a linear rise in ΔP with filtration time (cf., Fig. S1b in the SI). The assumption that the cake covers the entire membrane surface area cannot be strictly true at very short filtration times, before a cake layer has deposited. The time required for deposition of the first layer of foulants depends on the permeate flux. At long filtration times, when the membrane surface has been covered, cake filtration is expected to be the dominant fouling mechanism.

3.4. Standard pore blocking

In contrast to the previously described fouling mechanisms, standard pore blocking assumes fouling occurs inside the membrane pores rather than on the surface [1].

Laminar flow through a straight cylindrical pore can be described using the Hagen-Poiseuille equation [1,14]:

$$Q \quad N\left(\frac{\pi r \quad \Delta P}{8\mu}\right) \tag{19}$$

where N is the number of membrane pores, r is the pore radius [m], and L is the pore length (*i.e.*, membrane thickness) [m].

If the initial and final flowrates are equal, the relationship of ΔP_t to ΔP_o is a function of the initial radius, r_o, and the radius at time t, r_t.

$$\Delta_t \quad \left(\frac{r}{r_t}\right)^4 \Delta \tag{20}$$

Following Hermia, a solids mass balance yields [1]:

$$N\pi \quad r_0^2 - r_t^2)L \qquad V \tag{21}$$

where C is the volume of particles deposited per unit volume of filtrate.

Rearranging Eq. (21) yields the desired ratio:

$$\left(\frac{r_t}{r}\right)^4 \quad \left(1 - \frac{V}{N\pi Lr^2}\right)^2 \tag{22}$$

Defining the constant for standard pore blocking K_s [m^{-3}] as:

$$K_s \quad \frac{}{N\pi Lr^2} \tag{23}$$

Substitution of Eq. (22) into Eq. (20) gives:

$$\Delta P_t \quad \frac{\Delta P_0}{1 - K_s a_o \quad t)^2} \tag{24}$$

which is the time dependence of ΔP for standard pore blocking.

Standard pore blocking occurs inside the pores, so it is not influenced by crossflow induced forces. Consequently, Eq. (24) is valid for both XFLOW and DEF operations. In Eq. (24), $K_s a_o\ t$ is always positive. Therefore, when $K_s a_o\ t$ is between 0 and 1, the denominator will be smaller than 1 and a rise in ΔP with time is predicted. When $K_s a_o\ t$, all the pores have been blocked, and ΔP increases to infinity.

Similar to complete pore blocking, a breakdown of the constant flux assumption occurs when all pores have been blocked by foulants. A correction should be made to account for removal of foulants inside the pore. As the pore radius decreases, the filtrate velocity through the remaining open area must increase to maintain constant flux. An increase in velocity will translate to stronger shear forces, which may remove previously deposited particles. Such a correction is beyond the scope of this paper, as standard pore blocking is much more likely to be significant under conditions where the foulant particle size is smaller than the pore diameter, which is not the case for the work reported here.

4. Experimental

4.1. Materials

PES-10 poly (ether sulfone) flat sheet UF membrane rolls were purchased from Nanostone Water (Eden Prairie, MN). Trizma HCl and potassium chloride (KCl) were purchased from Sigma Aldrich (St. Louis, MO). Sodium hydroxide (NaOH) and denatured ethyl alcohol were purchased from Fisher Scientific (Pittsburgh, PA). Buffer solution with a pH of 6 was purchased from Fluka Analytical (Munich, Germany). Soybean oil (Wesson) was obtained from a local supermarket. Xiameter OFX-0193 non-ionic, silicone-based surfactant was purchased from Dow Corning (Midland, MI). A latex microsphere suspension containing 10 wt□ polystyrene particles (diameter: 0.22 μm) was purchased from Thermo Scientific, Inc. (Fremont, CA). All chemicals were used as received. Ultrapure water (18.2 MΩ-cm at 25 °C, 5 ppb TOC) was obtained from a Millipore Milli-Q Advantage A10 water purification system (Billerica, MA).

4.2. Membrane pretreatment

20 cm × 28 cm flat membrane sheets were cut from a PES-10 roll. Membrane sheets were immersed in a dish of ethanol for 24 h with the active layer facing down to wet the porous structure of the membrane. The membranes were then soaked in ultrapure water for another 24 h to displace the ethanol from the pores. Pretreated membranes were stored in ultrapure water until use.

4.3. Foulant preparation

Two foulant mixtures were used throughout this study: 200 ppm 0.22 μm latex bead suspensions and 200 ppm soybean oil emulsions.

The latex bead suspension was made by first carefully rolling the latex bead container on a flat surface, followed by sonication in a bath for 30 s to uniformly disperse the latex beads. 16 g of 10 wt□ latex bead suspension (0.22 μm) were diluted with 8 L of ultrapure water. The ionic strength was adjusted to 10^{-5} M using 80 μL of 1 M KCl solution. The pH of the suspension was adjusted to 6 using 8 mL of pH 6 buffer [18].

The soybean oil emulsion was prepared by mixing 1.44 g soybean oil and 0.16 g OFX-0193 surfactant with 1 L of ultrapure water. This solution was blended vigorously using a commercial heavy duty blender (Waring Laboratory, Stamford, CT) at 20,000 rpm for 3 min. The emulsion was then diluted with another 7 L of DI water. Oil droplets had an average diameter of ~3.4 ± 1.3 μm [18].

4.4. Constant flux crossflow fouling experiments

Details of the crossflow system are provided elsewhere [19]. Crossflow cells had a rectangular flow path 31.75 mm wide × 82.55 mm long × 2.565 mm deep [19]. Three membrane samples (filtration area of 19.4 cm^2) were tested simultaneously during each run. The feed flow rate was set to 0.8 L/min, corresponding to a crossflow velocity of 0.164 m/s and a Reynolds number of ~1000. The Reynolds number was calculated by approximating the channel as two parallel plates and using channel height as the characteristic dimension [19]. Feed pressure was set to 30 psig (~2.1 barg). These conditions were used for all crossflow experiments. The permeate flux of each cell was controlled by a dedicated peristaltic pump (Cole-Parmer, Vernon Hills, IL). The permeate flow rates were measured by Coriolis-type flow meters (Bronkhorst, Bethlehem, PA) downstream from the peristaltic pumps. Flow meters and pumps were connected to a PC running LabVIEW®. A PID controller in the program adjusted the voltage to the permeate pumps to maintain the permeate flux set-point. Initially, the operating parameters (*i.e.*, feed flow, feed pressure, and permeate flux) were adjusted to their desired values with DI water flowing through the system. Fouling was initiated by switching the feed inlet from the DI water tank to the foulant tank. To avoid dilution of the foulant with DI water present in the system, the solution was directed to the drain until it visibly looked like the fresh fouling solution, at which point both permeate and effluent streams were recycled back to the foulant feed tank. As the membranes fouled, the ΔP required to maintain the desired constant flux increased due to increasing mass transfer resistance. Differential pressure transducers monitored the ΔP in each cell over time.

The TF was measured by flux stepping, a technique commonly used in the literature [11,12,20]. Membranes were first challenged with foulant at a low (*i.e.*, 20 LMH), constant flux for 20 min, and then the permeate flux set-point was increased by 10 LMH every 20 min. The experiment was terminated when ΔP reached 30 psig (*i.e.,* equal to the feed pressure), because ΔP larger than the feed pressure may lead to formation of air bubbles in the permeate line, disrupting the control loop. From the experiments, a numerical value of the TF of each foulant-membrane pair was determined as described below.

Constant flux crossflow fouling experiments were similar to flux stepping experiments, except the permeate flux was set to a fixed value rather than increasing during the experiment. Permeate and feed samples were collected only during constant flux experiments which ran longer than 30 min, allowing the permeate line to be completely filled with fresh permeate. For the soybean oil emulsion, membrane rejection was determined from total organic carbon (TOC) analysis. TOC values of permeate and feed samples were measured using a total organic carbon analyzer from Shimadzu Scientific (Japan). Rejection was calculated as follows:

$$R \quad \left(1 - \frac{p}{f}\right)\cdot 100 \tag{25}$$

where R is the percent rejection, and C_p and C_f are the organic carbon concentrations in the permeate and feed, respectively.

Latex bead suspension rejection was based on turbidity using a Hach2100AN turbidity meter (Loveland, CO). Feed and permeate turbidities were measured, and the rejection was calculated using Eq. (25), substituting turbidity for organic carbon concentration.

4.5. Pure water permeance

The pure water permeance of samples tested in the crossflow system was calculated online by LabVIEW® software as follows:

$$\text{Permeance} \quad \overline{\Delta P} \tag{26}$$

The permeate flux was measured by Coriolis flow meters downstream of the permeate pumps. ΔP was measured using differential pressure transducers on each cell. To minimize errors caused by fluctuations in the measured ΔP, the pure water permeance of a sample was taken as the average of all permeance measurements taken in the 30 s prior to initiating fouling.

5. Results and discussion

5.1. Constant flux crossflow fouling experiments

Constant flux crossflow fouling experiments were conducted at permeate fluxes ranging from 20 LMH to 130 LMH in intervals of 10 LMH. For brevity, we present representative results here, with all additional experimental results provided in Fig. S2 in the SI. Latex bead suspensions are often used as model foulants in fouling research [21–23], and are ideal for our purposes due to the model assumptions of uniform, spherical, non-deformable foulant particles. In practice, foulants often do not meet these restrictions. For example, emulsified oil droplets, found in hydraulic fracturing wastewater, are deformable and can coalesce into larger droplets [15]. To investigate whether this property affects the applicability of fouling models to this class of foulants, latex bead suspensions and soybean oil emulsions were used to model non-deformable and deformable foulants, respectively.

ΔP was recorded as a function of filtration time. To minimize the effect of permeance variation on model parameters, membrane samples selected for constant flux crossflow experiments had permeance values as close to each other as possible. Membrane samples used with the latex bead suspension had permeance values ranging from 221 to 238 LMH/bar, with an average permeance of 228 ± 5 LMH/bar. Membrane samples used with the soybean oil emulsion had permeance values ranging from 227 to 238 LMH/bar, with an average permeance of 234 ± 4 LMH/bar. Latex bead rejection was 100□. Soybean oil rejection was 98.7 ± 0.3□. Representative results of the constant flux experiments for both foulants are presented in Fig. 3.

As permeate flux increases, the ΔP of both foulants changes very slowly with time at low flux and more rapidly at higher flux, particularly above the TF. The TF is the flux below which the membrane fouls slowly and above which the membrane fouls rapidly [10,13]. As discussed in more detail below, TF values were measured for both foulants using flux stepping experiments. The latex bead suspension had a TF value of ~80 LMH, and the soybean oil emulsion had a TF value of ~50 LMH. The qualitative behavior of the ΔP profiles can be divided into three regions: below the TF, near but below the TF, and above the TF. Changes in the time dependence of the ΔP profiles with permeate flux can be attributed to fouling mechanism changes. Even at the lowest measured permeate flux some fouling was observed. Therefore, critical flux values could not be measured for these systems [10,24].

Fig. 3a presents data for experiments conducted with the latex bead suspension. Far below the TF for this foulant (*i.e.*, 30–50 LMH), ΔP increases initially and then approaches a plateau with filtration time (cf., Fig. 4a). This profile is similar to the theoretical profile predicted for fouling by the intermediate pore blocking mechanism (cf., Fig. S1a in the SI). As the permeate flux approaches the TF for this foulant (*i.e.*, 60–70 LMH), ΔP displays a more rapid initial increase with time, and at long filtration times, ΔP continues to rise gradually with time. This gradual rise in ΔP is similar to the theoretical profile predicted for fouling by the cake filtration mechanism (cf., Fig. S1b in the SI). Above the measured TF for this foulant (*i.e.*, 90–110 LMH), there is a sharp increase in ΔP followed by an abrupt transition to a slower rate of increase in ΔP with time. (cf., Fig. 4b).

The continual rise of ΔP with filtration time in the later part of the experiment is associated with cake accumulation, implying that the foulant cake continues to grow indefinitely. In contrast, during constant ΔP filtration, permeate flux declines, and the cake reaches a constant thickness. Jiao and Sharma showed that the size of particles that can deposit onto the cake decreases as permeate flux declines, until there are no available particles small enough to deposit on the cake [25]. In constant flux filtration, foulant particle size distribution can affect the cake density, but it is not expected to vary significantly with time (*i.e.*, the size of particles that can deposit onto the cake is invariant with time). Evidence for this is the near linear increase in transmembrane pressure observed during the later stages of fouling experiments above the threshold flux. Foulant particle rigidity can play a more significant role, as deformable particles (*e.g.*, oil droplets) can coalesce.

Fig. 3b presents experimental results for the soybean oil emulsion. At permeate fluxes approaching the TF of this foulant (*i.e.*, 30–40 LMH), ΔP profiles are similar to those of the latex bead suspension near but below its TF, exhibiting an initial ΔP increase followed by a region of slower ΔP rise. However, above the TF of the soybean oil emulsion (*i.e.*, 60–80 LMH), the transition between the initial ΔP increase and the slow ΔP rise region is more gradual. As a result, the ΔP profiles of the soybean oil emulsion do not display the "kink" seen in the latex bead suspension ΔP profiles.

The difference between the ΔP profiles of the latex bead suspension

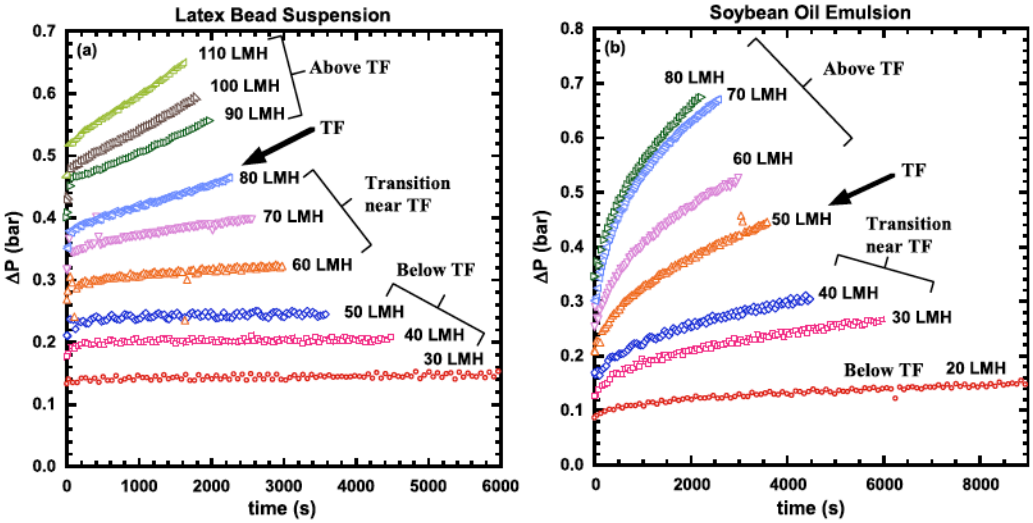

Fig. 3. Influence of filtration time on ΔP in constant flux fouling experiments conducted with: (a) 200 ppm 0.22 μm latex bead suspension and (b) 200 ppm soybean oil emulsion. TF - Threshold Flux.

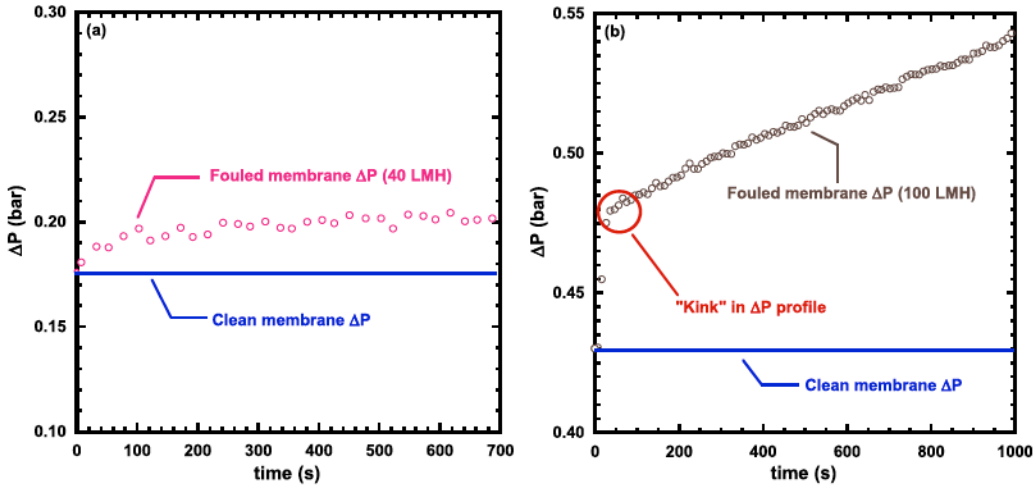

Fig. 4. Influence of filtration time on ΔP in constant flux fouling experiments conducted with 200 ppm 0.22 μm latex bead suspension: (a) close-up view of ΔP behavior at 40 LMH (below the TF), (b) close-up view of ΔP behavior at 100 LMH (above the TF).

and the soybean oil emulsion above the TF may be due to at least two phenomena. First, in contrast to the latex bead suspension, rejection of the soybean oil emulsion by the membrane is not complete. At high fluxes, emulsified oil droplets have been shown to deform and "squeeze" through membrane pores, despite originally having a diameter larger than that of the membrane pores [15]. Second, the drag force on the droplets can cause them to coalesce into larger droplets, which are more easily removed from the surface of the membrane by the crossflow shearing force [15]. These two phenomena result in foulant removal from the membrane surface, perhaps moderating the increase in ΔP, smoothing the transition from intermediate pore blocking behavior to more cake filtration-like behavior.

To summarize, ΔP profiles from constant flux experiments (especially for the latex bead suspension) suggest a transition between two mechanisms of fouling. Initially, fouling is dominated by intermediate pore blocking. Following the initial increase in ΔP with time (attributed to intermediate pore blocking), the ΔP profiles change based on permeate flux. At low fluxes (relative to the TF), the ΔP profile plateaus, as predicted by intermediate pore blocking (cf., Fig. S1a in the SI). At high fluxes (relative to the TF), the rate of ΔP increase decreases, but it reaches a region of approximately linear ΔP rise, which is more consistent with cake filtration (cf., Fig. S1b in the SI).

5.2. Combined intermediate pore blocking and cake filtration model

Based on the above observations, a model combining intermediate pore blocking and cake filtration was proposed to describe the fouling results presented in Fig. 3. Standard pore blocking is expected to play a modest role because the size of the particles (0.22 μm latex beads and ~3.4 μm oil droplets [18]) is much larger than the nominal membrane pore diameter (~3 nm, measured by molecular weight cutoff experiments as detailed in Section 3 of the SI) and the high rejections (100□ for latex beads and > 98□ for oil droplets).

The combined model considers fouling to occur by both mechanisms simultaneously. Initially, intermediate pore blocking is the dominant mechanism, transitioning over time to cake filtration. Eq. (11) describes the reduction in unobstructed membrane surface area as the membrane initially fouls by intermediate pore blocking. During this initial intermediate pore blocking stage, the overall filter resistance is assumed to be constant, due to negligible cake growth. Eq. (16) describes the increase in total resistance as foulant layers accumulate on the membrane due to cake buildup. Comparing the initial and final flowrates using Darcy's Law (Eq. (1)) and substituting in Eqs. (11) and (16) results in:

$$\Delta P_f = \frac{\Delta P_0 \quad 1 \quad K_c J t)}{\left(\frac{1}{K_i} \quad 1 - \frac{1}{K_i}\right)\exp\left(-K_i \quad t\right)\Big)} \tag{27}$$

which is the time dependence of ΔP for the combined model.

The term K_i in Eqs. (12) and (27) is the ratio of the stable ΔP at the end of the intermediate pore blocking stage to the initial ΔP. The intermediate pore blocking stage could be considered complete when most of the membrane surface area was covered with foulant, and this ratio may reflect the mass transfer resistance of a monolayer of foulant on the membrane surface. The ΔP at the end of the intermediate pore blocking stage is the initial ΔP for cake filtration. The minimum value of K_i is 1, representing either zero flux through the membrane or very high rates of foulant removal. In either case, fouling is negligible, and intermediate pore blocking does not contribute to ΔP.

K_c in Eqs. (12) and (27) represents the rate of accumulation of cake on the membrane. When K_c is very small (*i.e.*, $1 \quad K_c \; t) \approx 1$) Eq. (27) reverts to Eq. (13), the original intermediate pore blocking equation. If both K_i and K_c are at their minimum values, ΔP is constant and equal to ΔP_0.

At very short times, the numerator of Eq. (27) approaches one (*i.e.*, $1 \quad K_c \; t) \approx 1$), and Eq. (27) reduces to Eq. (13) for pure intermediate pore blocking behavior. At long times ($\rightarrow \infty$), the exponent in the denominator approaches zero (*i.e.*, $\exp -K_i \; t) \approx 0$) and Eq. (27) becomes:

$$\Delta P_f = \Delta P_0 K_i \quad 1 \quad K_c \; t) \tag{28}$$

As described in Section 3.2, the part of the equation representing intermediate pore blocking converges to a constant value of $\Delta P \quad _i$. Afterwards, ΔP increases linearly with time, following the cake filtration model. This time-dependent behavior is at least qualitatively consistent with the fouling progression observed in Fig. 3. Initially, the pristine membrane gets fouled according to the intermediate pore blocking mechanism. After some time has passed and enough foulant has accumulated on the membrane, ΔP becomes controlled by the rate of cake buildup. *En passant*, for microfiltration membranes, the initial fouling will be influenced by standard pore blocking as well, and this is a topic of ongoing research.

5.3. Modeling

Model fittings were done using Matlab R2017b® software by the least squares method (for a sample fitting script, see Section 4 of the SI). Several fitting strategies were attempted, and they are outlined in more detail in Section 5 of the SI. According to the combined model, ΔP

should rise approximately linearly later in the experiment, and the slope should equal $\Delta P\ K_i K_c$ (cf., Eq. (28)). Combining this expression for the slope and Eq. (12), K_c can be expressed in terms of B as follows:

$$K_c = \frac{slope \cdot}{\Delta P_o \quad \sigma J) J} \tag{29}$$

K_i and K_c were expressed in terms of B and σ using Eqs. (12) and (29), respectively, and the model was fit to experimental data by treating B as an adjustable parameter.

σ is expected to remain constant with flux (cf., Section 5 of the SI). To determine the optimum value for σ, a grid search method was used [26]. B was allowed to vary to fit the ΔP *vs.* time data for each flux, and the values of K_i and K_c were calculated according to Eqs. (12) and (29), respectively. σ values ranged from 0 to 600 m^{-1} (based on the three parameter fits described in the SI) in intervals of 50 m^{-1}. A sum of the fitting errors for all tested fluxes was calculated to determine the best value of σ.

The above description applies to the non-deformable latex beads. For the deformable oil droplets, σ is not expected to remain invariant with flux. As permeate flux increases, higher drag force is applied to the oil droplets, and they may "flatten" on the membrane surface, increasing their coverage area [27]. Therefore, both σ and B were allowed to vary during the second stage of fitting for the soybean oil emulsion fouling experiments.

As shown in Fig. 5, below the TF, most experiments can be fitted using only the intermediate pore blocking model. Above the TF, where cake filtration had a more significant impact, the experiments were fit with the combined model. As described in Section 5.1, as the permeate flux approaches the TF, there is a transition where ΔP profiles do not strictly obey the intermediate pore blocking model. Once the ΔP profiles started displaying a near linear increase in ΔP later in the experiment, K_c values began increasing rapidly with flux (cf., Fig. S4 in the SI), and the combined model was applied.

Fig. 5 compares the model fits with the experimental data for representative constant flux experiments. At fluxes well below the TF (*i.e.*, 20 and 40 LMH for the latex beads and 20 LMH for the soybean oil emulsion), both the intermediate pore blocking model and the combined model fit the data well. Fig. S5 in the SI compares the two fits below the TF, and the intermediate pore blocking model by itself is sufficient to describe the data. As the flux approaches the TF and rises above it (60, 80, 100 and 120 LMH for the latex beads, and 40, 60, 80, and 100 LMH for the soybean oil emulsion), the combined model is required for an accurate fit. For comparison, attempts were made to fit the experimental data using only the complete pore blocking (cf., Eq. (8)), intermediate pore blocking (cf., Eq. (13)) or cake filtration (cf., Eq. (18)) models (Fig. S6 in the SI). These fouling models were unable to accurately describe the experimental data, which supports the qualitative description of fouling proposed in Section 5.2. A discussion of the trends in the fitted parameter values with flux is presented in Section 5 of the SI.

5.4. Refining the definition of threshold flux

TF is often measured with a flux stepping experiment as described in Section 4.4 [20,28]. Flux stepping was originally developed to identify the onset of fouling in membrane bioreactor (MBR) systems [29]. Miller et al. adapted the method for constant flux crossflow fouling studies [11].

As discussed above, the intermediate pore blocking model describes the experimental data far below the TF, while near and above the TF, the combined model must be used. Therefore, we propose the following physical definition of the TF in constant flux crossflow filtration: *the flux below which cake buildup is negligible and above which cake filtration becomes the dominant fouling mechanism*. Below the TF, crossflow shear forces remove foulants at a rate which keeps the cake from growing thick enough to strongly influence ΔP. Above the TF, foulants deposit onto the membrane too quickly to be removed by crossflow shear, the cake grows and contributes significantly to the continuous rise in ΔP with filtration time.

Fig. 6a presents the results of a flux stepping experiment conducted with the latex bead suspension, as well as a simulation discussed below. Three common methods for determining the TF are reviewed below in the context of our proposed definition of TF. A more thorough explanation is provided through a mathematical analysis of each method, using the combined intermediate pore blocking and cake filtration model. Only the first step in the flux stepping experiment is affected by intermediate pore blocking, since only for that step is the membrane surface initially clean. Therefore, the mathematical analysis assumes fouling times long enough that Eq. (28) is the relevant fouling model.

5.4.1. d P)/dt

In this method, the rate of change in ΔP during each step is calculated. The value of d(ΔP)/dt for each step is plotted *vs.* permeate flux, and the TF is identified as the flux where d(ΔP)/dt begins to increase rapidly [11,20,29]. This method corresponds to the definition of the TF as marking the transition between slow and rapid fouling.

Taking the derivative with time of Eq. (28):

$$\frac{d\ \Delta P)}{dt} \quad \Delta P_0 K_i K_c \tag{30}$$

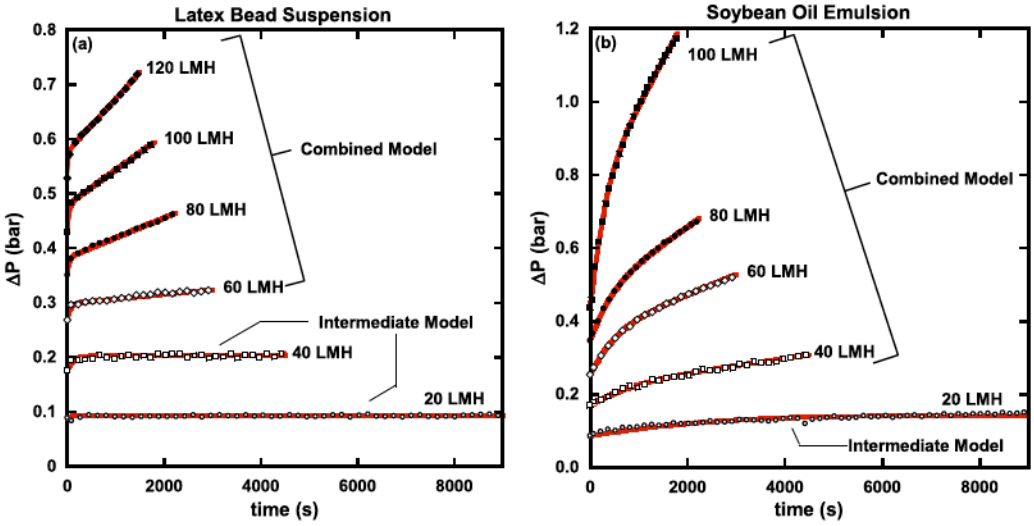

Fig. 5. Model fits for constant flux experiments conducted with: (a) 200 ppm 0.22 μm latex bead suspensions (TF ~80 LMH) and (b) 200 ppm soybean oil emulsions (TF ~50 LMH). Experimental data are shown with markers. Model fits are shown with red lines. (For interpretation of the references to colour in this figure legend, the reader is referred to the web version of this article.)

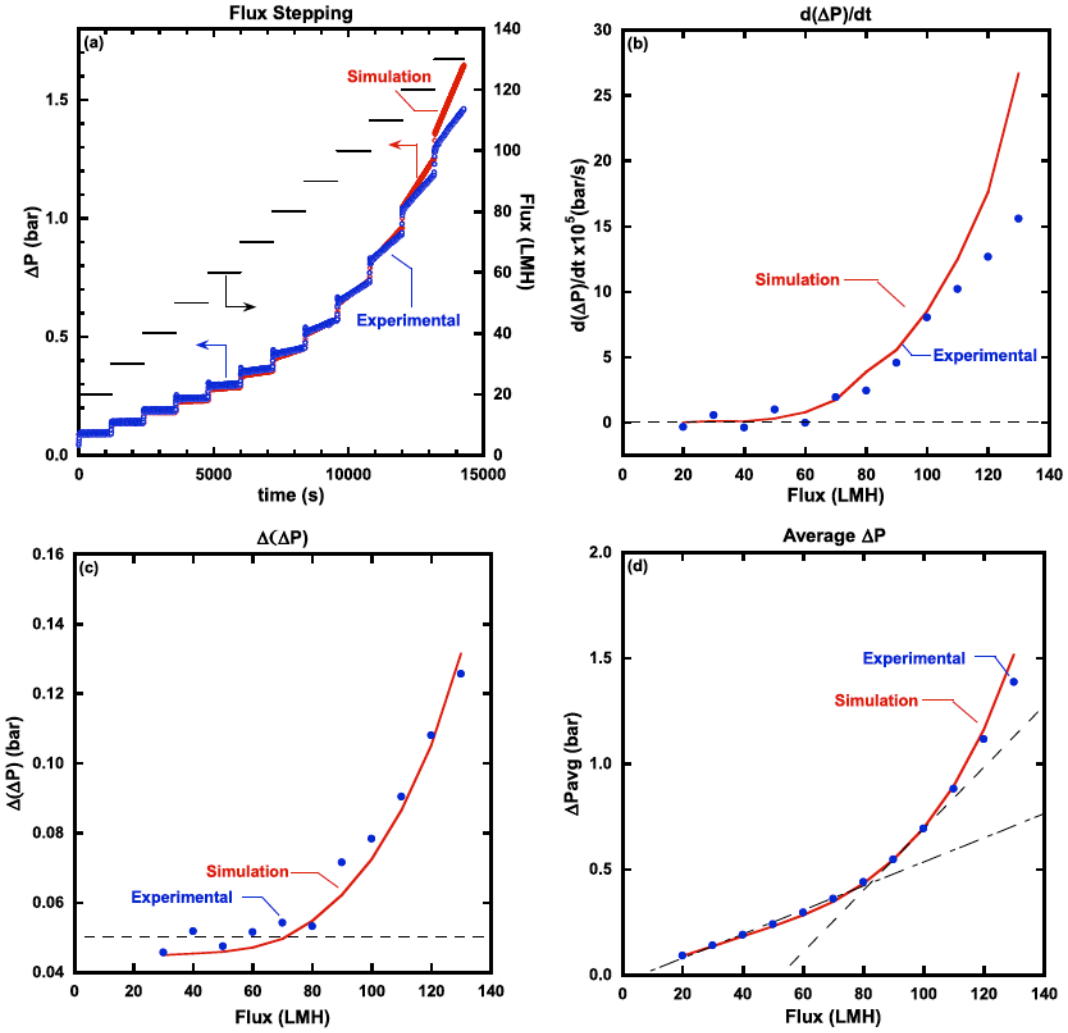

Fig. 6. Flux stepping experiments and analysis to determine TF: (a) ΔP and flux *vs.* time data for a flux stepping experiment conducted with a 200 ppm 0.22 μm latex bead suspension and a flux stepping simulation based on constant flux model fits. Analysis of experimental and simulated data using: (b) d(ΔP)/dt method, (c) $\Delta(\Delta P)$ method and (d) Average ΔP method.

Based on constant flux fitting results (cf., Table S2 in the SI), K_i for the latex bead fouling experiments was constant at ~1.1. The permeate flux is ≈ $10^{-5} m/s$). Consequently, when K_c is small (*i.e.*, negligible cake accumulation), d(ΔP)/dt ≈ 0. An increase in either permeate flux or K_c contributes to a rise in d(ΔP)/dt. In flux stepping, permeate flux increases in a step wise fashion, while d(ΔP)/dt remains more or less constant below the TF. Thus, a rapid increase in d(ΔP)/dt depends on an increase in K_c.

According to Table S4 and Fig. S4 in the SI, K_c values increase sharply from ~1 at 50 LMH to ~4.3 at the TF (80 LMH). This result is consistent with the experimental results shown in Fig. 6b, where d(ΔP)/dt values are near zero at low fluxes and begin to increase rapidly around 60 LMH. Above the TF, K_c begins to reach a plateau, as explained in Section 5.2 of the SI, and d(ΔP)/dt values increase more linearly with increases in permeate flux.

5.4.2. └ P)

When permeate flux increases in a flux stepping experiment, the ΔP profile shows a corresponding increase (cf., Fig. 6a). The permeate flux step is constant (10 LMH), so the increase in ΔP between steps should be constant if there is no change in fouling behavior. $\Delta(\Delta P)$ is calculated as the difference between the first ΔP measurement of step n + 1 and the last ΔP measurement of step n. In our experiments, the first measurement in step n + 1 is taken 120 s after the flux increase to give ΔP time to stabilize. $\Delta(\Delta P)$ values are then plotted *vs.* permeate flux, and the TF is identified as the flux where $\Delta(\Delta P)$ increases rapidly [11,20,29].

Using Eq. (28), the ΔP difference between the first measurement of step n + 1 and the last measurement of step n is:

$$\begin{aligned} \Delta\,\Delta P) &= \Delta P^{n\ 1}_{initial} - \Delta P^{n}_{final} \\ &= \Delta P^{n}_{0}\ {}^{1}K_i^{n\ 1}\ 1 \quad K_c^{n\ 1\ n\ 1}t^{n\ 1}_{initial}) - \Delta P^{n}_{0} K_i^{n\ 1} \quad K_c^{n\ n}t^{n}_{final}) \end{aligned} \tag{31}$$

At small values of K_c the second terms in the parentheses are negligible, and Eq. (31) becomes:

$$\Delta\,\Delta P) = \Delta P^{n\ 1}_{0\ \ i}{}^{n\ 1} - \Delta P^{n\ \ n}_{0\ \ i} \tag{32}$$

K_i is taken as a constant, as mentioned above. The initial ΔP of each step is replaced with the flux divided by the membrane permeance at the end of step n, $permeance^n$ (cf., Eq. (26)) (assuming a negligible change in permeance during the time between measurements):

$$\Delta\left(\Delta P\right) = K_i \frac{{}^{n\ 1} - {}^{n})}{permeance^n} \tag{33}$$

A value of 1.1 is used for K_i (see Section 5.4.1). The difference between consecutive flux steps is 10 LMH. During the first flux steps, fouling is low, and permeance is taken to be constant (~230 LMH/bar, which is the clean membrane permeance). Using these values,

$\Delta\ \Delta\ ) \approx 0.0478bar$. When K_c becomes large enough that the second terms in parentheses of Eq. (31) are not negligible, Δ begins to rise. This result is consistent with the experimental results shown in Fig. 6c. Below the TF, $\Delta(\Delta P)$ values are $\approx$ 0.05 bar, and they begin to increase around the TF (80 LMH).

5.4.3. Average P

The average ΔP for each flux step is calculated and plotted *vs.* permeate flux. A linear trend line is plotted through the data until the point where the R^2 value of the best fit of a line through the data is lower than 0.99 [12,30]. A second linear trend line is then plotted through the next two points. As shown in Fig. 6d, the TF is identified as the point of intersection of these two lines.

The running time average of ΔP, ΔP_{avg}, may be calculated by averaging Eq. (28) over a time interval Δt, as shown below:

$$\Delta P_{avg} = \frac{1}{\Delta t}\int_{t}^{t\ \Delta t} \Delta P_0 K_i\ 1\quad K_c\ t')dt' = \Delta P_0 K_i\left(1\quad K_c\ t\quad 0.5K_c\ \Delta t\right) \tag{34}$$

Substituting ΔP_O according to Eq. (26):

$$\Delta P_{avg} = \frac{K_i}{permeance}\left(\quad K_c\ ^2t\quad 0\ 5K_c\ ^2\Delta t\right) \tag{35}$$

For small values of K_c, Eq. (35) reduces to: $\Delta P_{avg}\quad \frac{K_i}{permeance}$. At low fluxes, fouling is low, and permeance is taken to be constant (~230 LMH/bar). Therefore, at low fluxes, ΔP_{avg} is a linear function of flux. For larger K_c values, ΔP_{avg} in Eq. (35) deviates from linearity. This result is consistent with the experimental results shown in Fig. 6d and with our proposed definition of the TF.

5.4.4. Threshold flux prediction

The proposed definition of TF is *the flux below which cake buildup is negligible and above which cake filtration becomes the dominant fouling mechanism*. This definition is consistent with the current empirical methods of identifying the TF discussed above. To support this point, a flux stepping experiment was simulated using the models set forth in this study. A detailed explanation of the simulation methodology is provided in Section 7 of the SI. In general, the first flux step was modeled using the intermediate pore blocking model, and subsequent steps were modeled using the cake filtration model, accounting for previous surface fouling. Fig. 6a compares the experimental ΔP measurements to the flux stepping simulation, which is based on parameters from fitting the models to constant flux fouling experiments (cf., Table S4 in the SI). Fig. 6(b–d) present comparisons of the three TF analysis methods using the experimental and simulated flux stepping data. Clearly, the simulation is at least qualitatively consistent with the experiments. At higher permeate fluxes (*i.e.*, 110–130 LMH) there is a more significant divergence between the simulation and experimental results. This deviation may be due to the effect of fouling history. The simulation is based on the fitted parameters from constant flux experiments, which are based on the fouling progression of a pristine membrane. In a flux stepping experiment, the surface has been gradually exposed to foulant at lower fluxes and some cake has accumulated prior to reaching high permeate fluxes. Cake packing may depend on permeate flux, and during the flux stepping experiment, the cake structure may evolve differently, thereby influencing fouling rates at higher fluxes. Fig. S7 in the SI presents a flux stepping simulation for the soybean oil emulsion. For soybean oil, the simulation is only accurate for fluxes below the TF, and it begins to deviate significantly from the experimental data above the TF.

Thus, for rigid particles the models could theoretically be applied to flux stepping data to predict the change in ΔP with filtration time during fouling. The first flux step is modeled only using intermediate pore blocking, and data from this experiment can be used to calculate K_i (Eq. (13)). In subsequent steps, the slope of each step can be calculated from the experimental data. Using the slope and K_i values, K_c for each step can be calculated (Eq. (28)). Although the combined model (Eq. (27)) requires the value of B, the duration of the initial rapid ΔP rise is typically short, and Eq. (28) should give a good estimate of ΔP during constant flux fouling.

6. Conclusions

A combined intermediate pore blocking and cake filtration model was developed to describe fouling of a poly(ether sulfone) ultrafiltration membrane by a 0.22 μm 200 ppm latex bead suspension or a 200 ppm soybean oil emulsion. Below the threshold flux, the intermediate pore blocking model correlated well with experimental data. Above the threshold flux, the combined intermediate pore blocking/cake filtration model gave the most accurate fits. Based on this observation, the following definition of the threshold flux is proposed: *the flux below which cake buildup is negligible and above which cake filtration becomes the dominant fouling mechanism*. Based on a mathematical analysis of the combined model, the model and the definition are consistent with empirical threshold flux determination methods. A flux stepping experiment was simulated using fitting parameters from constant flux crossflow fouling experiments. For rigid particles, the simulation matched the experimental flux stepping data closely. Analysis of flux stepping experiments using the proposed models could enable prediction of fouling behavior in constant flux fouling experiments.

Acknowledgements

The authors gratefully acknowledge financial support from the National Science Foundation (MRSEC under award number DMR-1720595) as well as partial support of this work by the Australian-American Fulbright Commission for the award to BDF of the U.S. Fulbright Distinguished Chair in Science, Technology and Innovation sponsored by the Commonwealth Scientific and Industrial Research Organization (CSIRO). The authors also acknowledge Prof. Mukul Sharma (UT Austin) for helpful discussions.

Appendix A. Supplementary material

Supplementary data associated with this article can be found in the online version at doi:10.1016/j.memsci.2018.12.001.

References

[1] J. Hermia, Constant pressure blocking filtration laws – application to power-law non-Newtonian fluids, Trans. Am. Inst. Chem. Eng. 60 (1982) 183–187.
[2] W.R. Bowen, J.I. Calvo, A. Hernández, Steps of membrane blocking in flux decline during protein microfiltration, J. Membr. Sci. 101 (1995) 153–165.
[3] C.-C. Ho, A.L. Zydney, A combined pore blockage and cake filtration model for protein fouling during microfiltration, J. Colloid Interface Sci. 232 (2000) 389–399.
[4] R.W. Field, D. Wu, J.A. Howell, B.B. Gupta, Critical flux concept for microfiltration fouling, J. Membr. Sci. 100 (1995) 259–272.
[5] R.W. Field, J.J. Wu, Modelling of permeability loss in membrane filtration: re-examination of fundamental fouling equations and their link to critical flux, Desalination 283 (2011) 68–74.
[6] M. Hlavacek, F. Bouchet, Constant flowrate blocking laws and an example of their application to dead-end microfiltration of protein solutions, J. Membr. Sci. 82 (1993) 285–295.
[7] C.-C. Ho, A.L. Zydney, Transmembrane pressure profiles during constant flux microfiltration of bovine serum albumin, J. Membr. Sci. 209 (2002) 363–377.
[8] G. Bolton, D. LaCasse, R. Kuriyel, Combined models of membrane fouling: development and application to microfiltration and ultrafiltration of biological fluids, J. Membr. Sci. 277 (2006) 75–84.
[9] The AWWA Subcommittee On Periodical Publications Of The Membrane Process, Microfiltration and ultrafiltration membranes for drinking water, J. Am. Water Works Assoc. 100 (2008) 84–97.
[10] R.W. Field, G.K. Pearce, Critical, sustainable and threshold fluxes for membrane filtration with water industry applications, Adv. Colloid Interface Sci. 164 (2011) 38–44.
[11] D.J. Miller, S. Kasemset, L. Wang, D.R. Paul, B.D. Freeman, Constant flux crossflow filtration evaluation of surface-modified fouling-resistant membranes, J. Membr. Sci. 452 (2014) 171–183.

[12] S. Kasemset, Z. He, D.J. Miller, B.D. Freeman, M.M. Sharma, Effect of polydopamine deposition conditions on polysulfone ultrafiltration membrane properties and threshold flux during oil/water emulsion filtration, Polymer 97 (2016) 247–257.
[13] A.Y. Kirschner, C.-C. Chang, S. Kasemset, T. Emrick, B.D. Freeman, Fouling-resistant ultrafiltration membranes prepared via co-deposition of dopamine/zwitterion composite coatings, J. Membr. Sci. 541 (2017) 300–311.
[14] R.W. Baker, Membrane Technology and Applications, Third ed., John Wiley & Sons Ltd, West Sussex, UK, 2012.
[15] E.N. Tummons, V.V. Tarabara, Jia W. Chew, A.G. Fane, Behavior of oil droplets at the membrane surface during crossflow microfiltration of oil–water emulsions, J. Membr. Sci. 500 (2016) 211–224.
[16] P. Le-Clech, V. Chen, T.A.G. Fane, Fouling in membrane bioreactors used in wastewater treatment, J. Membr. Sci. 284 (2006) 17–53.
[17] B.F. Ruth, Studies in filtration III: derivation of general filtration equations, Ind. Eng. Chem. 27 (1935) 708–723.
[18] Z. He, D.J. Miller, S. Kasemset, L. Wang, D.R. Paul, B.D. Freeman, Fouling propensity of a poly(vinylidene fluoride) microfiltration membrane to several model oil/water emulsions, J. Membr. Sci. 514 (2016) 659–670.
[19] D.J. Miller, D.R. Paul, B.D. Freeman, A crossflow filtration system for constant permeate flux membrane fouling characterization, Rev. Sci. Instrum. 84 (2013) 035003.
[20] B.S. Prip, J. Gunnar, Critical flux determination by flux-stepping, AIChE J. 56 (2010) 1739–1747.
[21] V.V. Tarabara, R.M. Hovinga, M.R. Wiesner, Constant transmembrane pressure vs. constant permeate flux: effect of particle size on crossflow membrane filtration, Environ. Eng. Sci. 19 (2002) 343–355.
[22] F. Zamani, H.J. Tanudjaja, E. Akhondi, W.B. Krantz, A.G. Fane, J.W. Chew, Flow-field mitigation of membrane fouling (FMMF) via manipulation of the convective flow in cross-flow membrane applications, J. Membr. Sci. 526 (2017) 377–386.
[23] H.P. Grace, Resistance and compressibility of filter cakes, Chem. Eng. Prog. 49 (1953) 303–318.
[24] Z.W. He, D.J. Miller, S. Kasemset, D.R. Paul, B.D. Freeman, The effect of permeate flux on membrane fouling during microfiltration of oily water, J. Membr. Sci. 525 (2017) 25–34.
[25] D. Jiao, M.M. Sharma, Mechanism of cake buildup in cross-flow filtration of colloidal suspensions, J. Colloid Interface Sci. 162 (1994) 454–462.
[26] P.R. Bevington, D.K. Robinson, Data Reduction and Error Analysis for the Physical Sciences, 3rd ed., The McGraw-Hill Companies, Inc., New York, NY, 2003.
[27] G. Fux, G.Z. Ramon, Microscale dynamics of oil droplets at a membrane surface: deformation, reversibility, and implications for fouling, Environ. Sci. Technol. 51 (2017) 13842–13849.
[28] P. Bacchin, P. Aimar, R.W. Field, Critical and sustainable fluxes: theory, experiments and applications, J. Membr. Sci. 281 (2006) 42–69.
[29] P. Le Clech, B. Jefferson, I.S. Chang, S.J. Judd, Critical flux determination by the flux-step method in a submerged membrane bioreactor, J. Membr. Sci. 227 (2003) 81–93.
[30] J. Luo, S.T. Morthensen, A.S. Meyer, M. Pinelo, Filtration behavior of casein glycomacropeptide (CGMP) in an enzymatic membrane reactor: fouling control by membrane selection and threshold flux operation, J. Membr. Sci. 469 (2014) 127–139.